Understanding Adsorption of Organics on Pt(111) in the Aqueous Phase: Insights from DFT based Implicit Solvent and Statistical Thermodynamics Models.

Gabriel A. Bramley,[†] Manh-Thuong Nguyen,[‡] Vassiliki-Alexandra Glezakou,[‡] Roger Rousseau,[‡] and Chris-Kriton Skylaris[*,†]

[†]*School of Chemistry, University of Southampton, Southampton SO17 1BJ, U.K.*

[‡]*Physical Sciences Division, Pacific Northwest National Laboratory, Richland, Washington 99352, United States*

E-mail: C.Skylaris@soton.ac.uk

Phone: (023) 8059 9381

Abstract

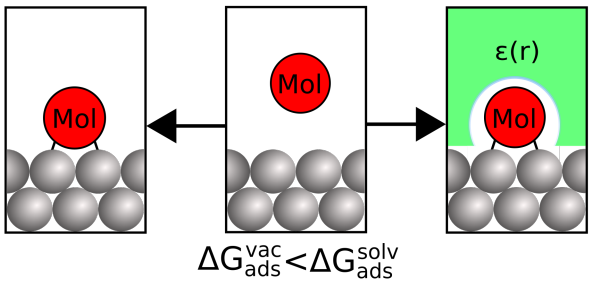

Adsorption of organics in the aqueous phase is an area which is experimentally difficult to measure, while computational techniques require extensive configurational sampling of the solvent and adsorbate. This is exceedingly computationally demanding,

which excludes its routine use. If implicit solvent could be applied instead, this would dramatically reduce the computational cost as configurational sampling of solvent is not needed. Here, using statistical thermodynamic arguments and DFT calculations with implicit solvent models, we show that semi-quantitative values for ΔG^{aq}_{ads} and ΔS^{aq}_{ads} for small organics can be calculated, for a range of coverages. We parameterise the soft sphere based solute dielectric cavity to an approximated free energy of solvation for a single Pt atom at the (111) facet, forming an upper and lower bound based on the entropy of water at the aqueous metal interface ($\Delta G_{solv}(Pt) = -4.35$ to -7.18 kJmol^{-1}). This captures the decrease in ΔG^{solv}_{ads} compared to ΔG^{vac}_{ads}, while solvent models with electron density based cavities fail to do so. For a range of oxygenated aromatics, the adsorption energetics using horizontal gas phase geometries significantly overestimate ΔG^{solv}_{ads} compared to experiment by ~ 100 kJmol^{-1}, but agree with *ab initio* MD simulations using similar geometries. This suggests oxygenated aromatic compounds adsorb perpendicular to the metallic surface, while the ΔG^{aq}_{ads} for vertical geometries of furfural and cyclohexanol agree to within 20 kJmol^{-1} of experimental studies. The proposed techniques provide an inexpensive toolset for validation and prediction of adsorption energetics on solvated metallic surfaces, which could be further validated by the future availability of more experimental measurements for the aqueous entropy/free energy of adsorption.

1 Introduction

Adsorption free energies (ΔG_{ads}) play an important role in determining the overall thermodynamics of heterogeneous catalytic processes. Competitive adsorption between different species dictates their relative coverages at the metallic surface, leading to reaction bottlenecks if the thermodynamic equilibrium favours the adsorption of one species over another.[1,2] However, enthalpic and entropic contributions to the free energy are altered by the presence of solvent (ΔG^{aq}_{ads}).[3] For example, solvent effects decrease ΔG^{aq}_{ads} of phenol to the Pt(111)

surface relative to ΔG_{ads}^{vac} from -220[4] to -29 kJmol^{-1}.[5] This results from the ΔH_{ads}^{aq} penalty of displacing the aqueous solvent layer, which is reduced by ΔS_{ads}^{aq} gain from the desorption of water into the liquid phase. Combined with further factors such as coverage,[4,6] the accurate calculation of ΔG_{ads}^{aq} requires understanding of the entropic and enthalpic contributions to the constituent steps of the adsorption process.

In atomistic simulations, implicit solvent methods provide a computationally inexpensive alternative to dynamic sampling techniques for calculating the free energy of solvation (ΔG_{solv}). In this method, the molecule is inserted into a cavity within a bulk dielectric medium, where ΔG_{solv} is calculated as a sum of: 1) polar contributions arising from the electronic response to the dielectric medium (ΔG_{pol}), and 2) non-polar contributions such as cavitation and dispersion-repulsion interactions, usually approximated from the shape and size of the cavity (ΔG_{npol}).[7] Many studies have been conducted to assess the quantitative accuracy of implicit solvent techniques with respect to experiment and explicit solvent simulations - particularly for proteins[8,9] and small molecules[10].[11] For large assays of solutes, the implicit solvent technique provides solvation free energies with errors of approximately 13.4 kJmol^{-1} (Generalised Born/SASA)[11] to 4.3 kJmol^{-1} (SMD).[10] In protein studies, publications also assess the structural accuracy of implicit solvent techniques, where the continuum solvent approach can lead to structural errors,[9] as well as spurious bottlenecks in the potential energy landscape for protein folding simulations.[8] In contrast, systematic quantitative studies for implicit solvation are rare for the adsorption process at metallic surfaces,[5,12] meaning thorough theoretical and experimental validation is required to perform predictive studies.[13]

At the metallic surface, large errors of ΔG_{solv} occur with electron density isovalue based dielectric cavity functions,[14] which mainly arise from the use of a single charge isocountour for species which require distinct cavity parameters (ie. heavy metallic and light organic atoms).[14,15] The optimal parameters for the solvation of small hydrocarbons dramatically undersolvate Pt atoms at the (111) facet, which require much smaller cavities to give accu-

rate values of ΔG_{solv}. This results in small ΔH_{solv} values compared to experimental binding enthalpies of aqueous solvent to Pt (-0.24 kJmol^{-1} [14] vs. -9.61 kJmol^{-1} [16] per atom). Consequently, anomalous values of ΔG^{aq}_{ads} arise, yielding either no improvements in the accuracy of adsorption free energies over standard vacuum calculations[17] or increased stabilisation of adsorption in solvent. In the case of phenol, this leads to ΔG^{aq}_{ads} errors of up to 200 kJmol^{-1} for the implicit solvent model vs. Cyclic Voltammetry experiments.[5] However, in this study, we will demonstrate that this inaccuracy is alleviated by separate parameterization of the metallic surface atoms and the organic adsorbates, leading to semi-qualitative agreement with experimental values of ΔG^{aq}_{ads} by decreasing the cavity size for the metallic atoms while maintaining the cavity parameters for the organic adsorbates.

In addition to constructing an implicit solvent model which accurately calculates ΔG^{aq}_{ads}, we will explore the ability of statistical mechanics based models to calculate ΔS^{aq}_{ads}.[18] In the gas phase, experiment has determined that the entropy of adsorbed species with strong lateral attractions ($\mathrm{S}^{\mathrm{gas,0}}_{\mathrm{ads}}$) follow a linear relationship with its 3D ideal gas entropy ($\mathrm{S}^{\mathrm{gas,0}}_{\mathrm{ads}}$),[19]

$$S^{gas,0}_{ads} = 0.68(S^{0}_{gas} - S^{0}_{gas,1D-trans}) \tag{1}$$

Where $S^{0}_{gas,1D-trans}$ is the standard molar entropy of the translational gas phase entropy. As $S^{gas,0}_{ads}$ is approximately 2/3 of S^{0}_{gas}, it is assumed many adsorbates follow a free translator (FT) regime, meaning 2D ideal gas models can approximate $S^{gas,0}_{ads}$.[20] Compared to more sophisticated lateral translational entropy expressions such as the Hindered Translator (HT) model, FT forms an upper bound where all translational microstates in the xy-plane are equally accessible. However, for flat potential energy which surfaces allow facile diffusion, comparisons of FT with Complete Potential Energetic Sampling (CPES) methods provide estimates of $S^{gas,0}_{ads}$ within 10 % of full sampling techniques for a range of temperatures above 273 K.[21] To calculate the entropy of solvation, simple models using empirical properties based on SPT (Scaled Particle Theory) and the accentric factor model accurately calculate the

ΔS^{3D}_{solv} of small molecules.[18] Using comparisons to experimental data, we will assess whether these simple geometric models based on statistical mechanics can provide approximate values for the entropy of solvation, and therefore the overall ΔS^{aq}_{ads}.

The role of coverage effects on the ΔG^{aq}_{ads} of small organics on metallic surfaces must also be understood to assess the accuracy of the implicit solvent model.[6] Although the decrease of adsorption enthalpy due to lateral repulsions between neighbouring adsorbates is observed in vacuum,[4,6,22] less is known about the impact of coverage for a solvated surface. Experimental data fit to the Femkin isotherm shows that ΔG^{aq}_{ads} has a weak dependence on coverage, with only a small decrease of 0 to 5 kJmol^{-1} from zero to full coverage for various organic molecules on the Pt(111) surface.[5,23] In contrast, ΔH^{vac}_{ads} decreases by 121 kJmol^{-1} over the same coverage range for phenol.[4] It has been proposed that phenol forms islands of high coverage in solvent, even at low concentrations, which emulates the effect of saturation coverage in vacuum. This can rationalise the seemingly low binding energies of phenol at the Pt(111) surface in the aqueous phase, but this theory has not been confirmed.[24] As the implicit solvent simulates the energetics of solvation, we will use this computationally affordable method to assess the coverage dependencies in the aqueous phase and evaluate the local high coverage theory. In addition, we will test different orientations of adsorbates at the Pt(111) surface to determine which geometries best match experimental energetics of adsorption.

In this study, we first validate the approach of separately parameterising the metallic surface atoms by comparing our results obtained with a commonly utilised electron density based formulation of the implicit solvent model. Then, using the increasing quantity of experimental reference data for the aqueous adsorption free energies of organics at the Pt surface[5,23,25] paired with older literature data,[26] we provide a quantitative analysis of ΔG^{aq}_{ads} values obtained with the Poisson-Boltzmann implicit solvent model for the Pt(111) surface. The validation of this new approach is achieved through comparisons to experimental data obtained from CV hydrogen underpotential deposition[5,23] and radio tracer[26] experiments,

which will allow for error estimations of ΔG_{ads}^{aq} in implicit solvent. We will also use statistical mechanics approximations for the solvation entropy[7,18] to facilitate further comparsion with experiment. Finally, we will investigate the ability of the implicit solvent model to capture the coverage dependency of ΔG_{ads}^{aq}. This will be achieved by performing simulations over a range of coverages with implicit solvent comparing their trends with experiment.

2 Methodology

2.1 *Ab initio* Simulations

Ab initio simulations were performed with the ONETEP[27] software package, which performs linear-scaling DFT simulations using localised non-orthogonal generalised Wannier functions (NGWFs)[28] with a basis of periodic sinc (psinc) functions. Simulations were performed using the Ensemble DFT (EDFT) method,[29,30] adapted to the localised NGWF framework of ONETEP by *Ruiz-Serrano et al.*,[31] and further developed to include Pulay mixing of the Hamiltonians.

The optB88-vdW-DF1 functional is used throughout this work.[32] Core states are represented by the Projector Augmented Waves (PAWs)[33] of the GBRV pseudopotential library.[34] The valence shell of Pt is represented with 12 NGWFs with cut-off radii of 12.0 a_0 and an electronic configuration of $5p^6 6s^1 5d^9 6p^0$. The psinc kinetic energy cut-off was set to 850 eV throughout. Geometry optimisations were performed with a LBFGS algorithm,[35] using the universal sparse preconditioner[36] with a convergence threshold of $|\mathrm{F}|\mathrm{max} < 3\mathrm{x}10^{-3}\ \mathrm{E_h a_0^{-1}}$.

Using the example of a commonly used/conventional plane wave code of a charge based implicit solvent model, comparison calculations for the electron density based dielectric cavity method were performed using the VASP Plane Wave DFT code package[37–39] with the VASPsol implicit solvent application[40].[41] Single-point energy calculations in VASP used the optimised geometries from calculations of ONETEP. PAW pseudopotentials[33,42] were used to represent the core electrons. A kinetic energy cut-off of 450 eV was used. Energy mini-

mization was performed with the RMM-DIIS procedure using Kerker preconditioning.

In light of the two different kinetic energy cut-offs for VASP and ONETEP, we note that the cut-offs in each code are not completely analogous to one another. Firstly, VASP considers the plane wave cut-off in a sphere in reciprocal space, whereas ONETEP includes the plane waves in a cube. Secondly, ONETEP requires higher kinetic energy cut-offs than plane wave codes to achieve sufficient localisation of the NGWFs.[43]

2.2 Implicit Solvation

Implicit solvent calculations were performed using ONETEP's Poisson-Boltzmann (PB) implicit solvent module,[44] where solutions to the PB equation are calculated using the bespoke DL_MG multigrid parallel solver.[45] The free energy of solvation (ΔG_{solv}) is expressed as:

$$\Delta G_{solv} = \Delta G_{pol} + \Delta G_{npol} \tag{2}$$

where ΔG_{pol} is the electronic response of the molecule to the bulk dielectric and ΔG_{npol} is the non-polar contribution composed of the cavitation free energy and dispersion-repulsion contributions. ΔG_{npol} is calculated using a linear relationship between the Surface Assessible Surface Area (SASA) and the Surface Accessible Volume (SAV):

$$\Delta G_{npol} = (\alpha * \gamma)S + pV \tag{3}$$

where γ is the surface tension of the solvent (0.07415 Nm^{-1}), p is the solvent pressure (-0.00035 GPa) and α is an additional scaling factor used to improve the fit of ΔG_{npol} to the experimental values of ΔG_{solv} (0.86).

The dielectric cavity is defined using the Soft Sphere atomic radii based cavity functions

of *Fisicaro et al.*[10] In this model, the dielectric cavity is defined as:

$$\epsilon(\mathbf{r}_i, \{\mathbf{R_i}\}) = (\epsilon_0 - 1)\Bigg\{ \prod_i h(\{r_i^{vdW}, \Delta, f\}; \|\mathbf{r} - \mathbf{R}_i\|) \Bigg\} + 1 \tag{4}$$

where ϵ_0 is the bulk dielectric constant (78.65), and h is a set of continuous, atom centered distance-based functions defined between 0 and 1, expressed as:

$$h(\{r_{vdW}^i, \Delta, f\}; \|\mathbf{r} - \mathbf{R}_i\|) = \frac{1}{2}\left[1 + \mathrm{erf}\left(\frac{\|\mathbf{r} - \mathbf{R}_i\| - f r_i^{vdW}}{\Delta}\right)\right] \tag{5}$$

which is defined by paramters Δ (the smearing width of the dielectric cavity function), r_{vdW}^i (the cavity radius of atom i taken from the vdW radius set of *Alvarez*[46]), and f (the linear scaling factor), while taking $\|\mathbf{r} - \mathbf{R}_i\|$ as an argument (the distance between the position of point $\mathbf{r}$ and atom i $\mathbf{R_i}$). The scaling factor of f = 1.20 is used to minimize the MAE of a test set of 20 neutral molecules with respect to experimental values[47] (details about the ONETEP implementation can be found in the method section of ref[14]). Pt uses a van der Waals radius of (2.29 Å), and f is varied to match the experimental values of ΔG_{solv} of a single Pt atom of the (111) facet. We outline this process in Section 3.2. We model this approach on our previous publication, where f is varied to obtain the correct work function of the Pt(111) in solvent, which provides initial guidance in obtaining optimal values of ΔG_{solv}.[14]

The charge based implicit solvent model of VASPsol was used to compare against our implementation of the Fisicaro method. Default settings for the H_2O solvent were used. In contrast to the soft sphere method, the charge based cavity in VASPsol method is defined using the charge density, $n(\mathbf{r})$:

$$\epsilon(n(\mathbf{r})) = 1 + \frac{1}{2}\left(\frac{\ln\left(n(\mathbf{r})/n_c\right)}{\sigma\sqrt{2}}\right)\left(\epsilon_0 - 1\right) \tag{6}$$

where similar to the soft sphere model, the efrc defines a smoothly switching function between

0 and 1, but n_c defines the charge isocontour of the function where the erfc is 0.5, and σ defines the width of the switching function.

2.3 Calculation of ΔG_{ads}^{aq}

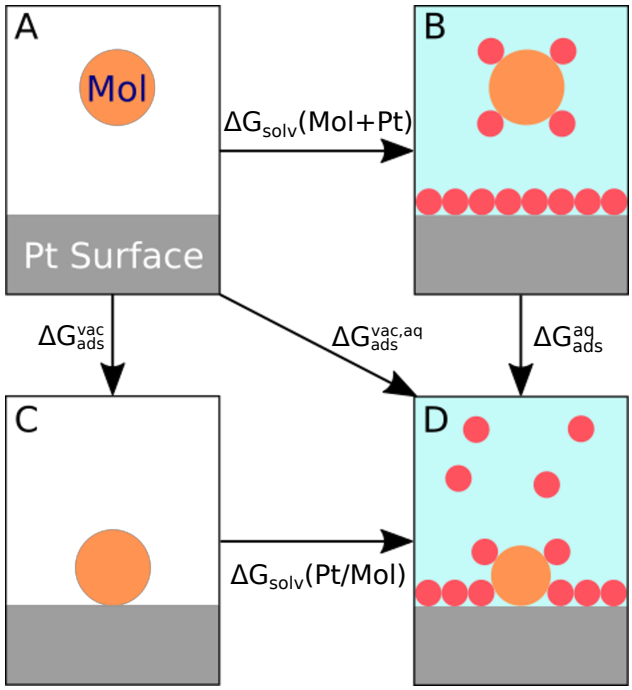

Figure 1: The process of adsorption according to four difference reference states is shown where A) The molecule and Pt(111) are isolated from one another in vacuum. B) Both the molecule and Pt(111) are isolated from one another in the solvent phase. C) The molecule is adsorbed onto the Pt(111) surface. D) The molecule is adsorbed onto the Pt(111) surface in the aqueous phase, which releases a number of water molecules into the aqueous phase relative to state B.

The adsorption free energy in the vacuum phase (ΔG_{ads}^{vac}) is calculated as the difference in free energies between the vacuum adsorbed system (M/Mol) and the isolated metallic slab and molecule (M+Mol):

$$\Delta G_{ads}^{vac} = G(M/Mol_{(vac)}) - (G(M_{(vac)}) + G(Mol_{(vac)}) \tag{7}$$

which corresponds to the free energy change between state A and C in the Hess Cycle of Figure 1. Assuming the overall entropy change for the $M_{(vac)}$ component of the system is

negligibly small, we can approximate ΔS^{vac}_{ads} solely through entropy changes experienced by the molecule, and ΔH^{vac}_{ads} through the 0 K total energy differences of the DFT calculations (equation 7). The entropy of the isolated molecule, $S(Mol_{(vac)})$ can be decomposed into translational, rotational, and vibrational components:[18]

$$S(Mol_{(vac)}) = S^{vac,3D}_{Mol} = S^{vac,3D}_{t} + S^{vac,3D}_{r} + S^{vac,3D}_{v} \tag{8}$$

$S^{vac,3D}_{v}$ is small compared to the other components, so we assume $\Delta S^{vac,3D}_{v,ads} = 0$. The method for calculating the translational and rotational terms is shown in the SI (Section S1). Alternatively, $S(Mol_{(vac)})$ could be taken as the empirical standard state gas phase entropy, but as our solvation entropies are calculated with analogous statistical mechanical approximations, we use the same method in the gas phase for the sake of consistency.

The entropy of the molecule adsorbed on the metallic surface is approximated using the 2D ideal gas approximation such that

$$S(M/Mol_{(vac)}) = S^{vac,2D}_{Mol} = S^{vac,2D}_{t} + S^{vac,2D}_{r} + S^{vac,2D}_{v} \tag{9}$$

where $S^{vac,2D}_{v}$ is again 0, and the entropy components are derived in the SI S2. In this approximation, it is assumed that the molecule can freely diffuse across the metallic surface, but is constrained to the xy-plane. We further assume this holds at high coverages, as noted by *Campbell et al.*[19] We note that the lost degrees of rotational freedom are potentially dependent on the binding mode of the molecule, especially in cases where non-yaw rotations would result in desorption (eg. phenol on Pt with four binding centres). This possibility will be explored in the results section.

Overall, ΔG^{vac}_{ads} is then calculated as:

$$\Delta G^{vac}_{ads} = (H(M/Mol_{(vac)}) - (H(M_{(vac)}) + H(Mol_{(vac)}))) - T((S^{vac,2D}_{Mol} - S^{vac,3D}_{Mol}) \tag{10}$$

where $S(M_{(vac)})$ is assumed to be negligable.

Calculating the free energy of adsorption under aqueous conditions (ΔG^{aq}_{ads}) requires further considerations. The implicit solvent calculates entropy components related to solvation within ΔG_{solv}, but the entropy of adsorption must be accounted for in a similar fashion to eq. 10. First, starting with the change of free energy from state B to D in Figure 1

$$\begin{aligned}\Delta G^{aq}_{ads} = (H(M/Mol_{(vac)}) - (H(M_{(vac)}) + H(Mol_{(vac)}))) \\ +(\Delta G_{solv}(M/Mol) - (\Delta G_{solv}(M) + \Delta G_{solv}(Mol))) \\ -T(S^{vac,2D}_{Mol} - S^{vac,3D}_{Mol})\end{aligned} \tag{11}$$

Where the first three terms represent the enthalpy of adsorption for a single point energy calculation, and the following three terms rerpesent the free energy changes of solvation calculated by the implicit solvent model, as expressed in equation 2. The change in entropy due to solvation are assumed to be included in the change of the ΔG_{solv}, therefore we assume in the last two term that the change of adsorption is equivalent to that of the gas phase.

Furthermore, we propose a simple method for calculating the overall entropy of adsorption using the solvation entropy methods of Garza and the 2D ideal gas model. The entropy in the solvent phase is calculated using the approach of *Garza*,[18] which adopts the 3D ideal gas equation to the entropy of solvation as:

$$S^{solv,3D}_{Mol} = S^{solv,3D}_{Mol,t} + S^{solv,3D}_{Mol,r} + S^{solv,3D}_{Mol,c} \tag{12}$$

where $S^{solv,3D}_{c}$ is the entropy of cavitation. A full derivation of terms is discussed in the Supporting Information (SI S3).

The overall entropy of adsorption in the aqueous phase is expressed as,

$$\Delta S^{aq}_{ads} = S^{solv,2D}_{M/Mol} - (S^{solv,3D}_{M} + S^{solv,3D}_{Mol}) \tag{13}$$

where $S_M^{solv,3D} = S_{M,c}^{solv,3D}$ and $S_{M/Mol}^{solv,2D}$ consists of the translational and rotational terms of $S_{Mol}^{vac,2D}$ and the cavitation term of the adsorbate and metal surface. The metal cavity volume (V_M) varies with the number of slab layers, which leads to a nonphysical dependence of $S_{M,c}^{solv}$ on N. Therefore, we consider the V_M for a single layer of Pt(111) only, and normalise by a factor of two so only one side of the slab is considered.

The packing factor of water ($\mathcal{G}(R_M, R_S)$, Equation S41, see SI) is different for metallic and organic solutes. Consequently, $S_{M/Mol,c}^{solv,2D}$ cannot be calculated directly, and $\Delta S_{ads,c}^{solv}$ is taken as the approximate cavity volume lost for the surface and molecule upon adsorption 12. For the metallic cavity, we multiply $S_{M,c}^{solv}$ per unit area by the cross sectional area of the M/Mol binding region. We approximate the area as the cross-sectional van der Waals' area of the molecule at the binding interface, A_{ov}. We calculate the loss of $S_{Mol,c}^{solv}$ upon adsorption as a proportion of the intersecting volume between the adsorbate and the metallic slab. Overall, we express gain of cavitation entropy as,

$$\Delta S_{ads,c}^{aq} = \frac{A_{ov}}{A_M} S_{M,c}^{solv,3D} + \frac{V_{int}}{V_{Mol}} S_{Mol,c}^{solv,3D} \tag{14}$$

where A_{ov} is the cross sectional area of the overlap between the metal and the adsorbate at the adsorption interface, A_M the cross-sectional area of the metallic slab, V_{int} is the overlapping volume of the metallic slab and adsorbate, and V_{Mol} is the van der Waals' volume of the molecule. All volumes are calculated using the van der Waals' radii of *Alvarez*.[46] For many molecules, it is feasible to simply approximate $\frac{V_{int}}{V_{Mol}} \approx 0.5$ if the species adsorbs horizontally, but the surface area approach allows for the exploration of alternative binding modes.

Overall, this yields the following expression for the entropy of adsorption in the aqueous phase.

$$\Delta S_{ads}^{aq} = S_{Mol}^{vac,2D} - (S_{Mol,r}^{solv,3D} + S_{Mol,t}^{solv,3D}) + \Delta S_{ads,c}^{solv} \tag{15}$$

where $S_{Mol}^{solv,3D}$ is separated out into translational and rotational components as the change

in cavitation is separated into $\Delta S^{solv}_{ads,c}$.

3 Results and Discussion

3.1 Entropy of Adsorption from First Principles

Campbell's Bond Additivity model treats the heats of adsorption of phenol to Pt(111) in the aqueous environment with a simple bond breaking/bond formation approach.[24] These calculations were enabled by recent experimental data, describing the bond energy of the Pt/H_2O interface, and enthalpies of adsorption and solvation for the molecule.

Akinola et al. explored an analogous approach for ΔS^{aq}_{ads}.[48] However, accuracy is limited by the lack of measurements for the entropy of solvation of the Pt(111) surface (ΔS_{solv}). *Akinola et al.*[48] inferred the value of ΔS_{solv} from the ice-like bilayer at the Pt/H_2O interface,[49,50] thereby approximating the entropy of adsorption as the entropy change of transition from liquid to the solid phase ie. the entropy of fusion (ΔS_{fus} = 25.1 $JK^{-1}mol^{-1}$[51]). We approximate the number of water molecules released upon adsorption by multiplying the cross-sectional area of the molecular binding interface (A_{ov} of equation 14) by the number of H_2O molecules per Pt atom (0.72[52]). We validate this for phenol through an AIMD simulation (SI S7), which predicts the displacement of 3.4 water molecules from the aqueous Pt(111) interface. This compares favourably to the surface area approximation which calculates the loss of 3.7 water atoms from the surface (Table 1).

However, water retains a significant amount of mobility at the Pt/H_2O interface at 298 K over a ps time scale,[53] meaning surface waters are expected to be more disordered than $H_2O_{(s)}$. As such, this value of ΔS_{solv} is interpreted as an upper bound. In contrast, the cavitation entropy calculated with either Scaled Particle Theory or the accentric factor method (SI S3) approximate the solvation entropy by assuming the adsorbed water retains the mobility of a solvation shell interacting with the solute via intermolecular forces (Equation S43).[18,54] However, relative to surfaces with weaker enthalpies of adhesion such as graphene,

water at the Pt(111) surface is more hindered, as indicated by its lower translational and rotational diffusion coefficients.[53] As a result, we can infer that the cavitation entropy calculated through the accentric cavity method acts as an informed lower bound for the entropy of solvation of the Pt atom. Establishing the above upper and lower bounds in this way allows us to better understand the expected ranged of values for ΔS_{solv}.

Table 1 shows that in all cases relative to the experimental data of ref.,[26] the entropy of cavitation approach predicts significantly lower $\Delta S_{ads,aq}$ values than electrochemical data. However, *Akinola et al.*[48] propose two major potential sources of error associated the experimental data of Table 1. First is the use of the HCl electrolyte, where Cl^- is known to bind to the Pt surface.[5,26,55] The co-adsorption of Cl^- to the surface is known to disrupt the packing and orientation of interfacial water, which introduces an error due to a dependence of the adsorbate binding energies on pH and voltage.[56,57] Secondly, the Van't Hoff linear regression covers a relatively small range of K_{eq} values (Between 1-2 over a range of 283-403 K), meaning.[48] The presence of these errors for $\Delta S_{ads,solv}$ is supported by substantially lower entropy values for studies performed with a weakly binding acetate buffer, which reduces the error due to electrolyte. For the adsorption of phenol on the Pt(100), Rh(111) and Rh(100) surfaces, the $\Delta S_{ads,aq}$ for Pt(100) is predicted to be $+59 \pm 39$ $JK^{-1}mol^{-1}$ relative to $+188$ $JK^{-1}mol^{-1}$ of *Bockris et al.* for Pt(111).[58] However, measurements with the acetate buffer still predict a high entropy value for phenol on the Pt(111) facet, but with a substantial error estimate ($+174 \pm 64 JK^{-1}mol^{-1}$). Further evidence shows that water on the Pt(100) and Pt(111) facets have similar dynamics and adhesion strength,[53] suggesting that increased ordering of water on the does not rationalise the large entropy differences between the two facets.

Nonetheless, the upper bound entropy calculated with the ice-like model closely agree with the higher values of $\Delta S_{ads,solv}$ measured with the HCl buffer across all molecules shown. Deciding which model better physically reflects adsorption at the solvated Pt surface requires more data measured with the acetate buffer. The large experimental errors associated with

the with the Van't Hoff approach for weakly adsorbing species adds further ambiguity. Therefore, it cannot be discounted that this agreement between the upper bound and experimental data of *Bockris et al.* is coincidental.

Values of $\Delta S_{ads,aq}$ show a strong correlation with the size of the molecule, varying between +93 $JK^{-1}mol^{-1}$ for benzene to +198 $JK^{-1}mol^{-1}$ for naphtholic acid. Entropy gain increases because of the greater number of desorbed waters from the metallic surface and loss of co-ordinating waters from the cavity of the molecule. This trend is also reflected in the experimental data. This correlation gives insight into the binding mechanism of the butanol and valeric acid. When bound horizontally, the $\Delta S_{ads,aq}$ of butanol/valeric acid are 37/35 $JK^{-1}mol^{-1}$ higher than experimental values respectively. However, when bound vertically to the surface via the oxygen atom, the trends observed for the other molecules is re-established - the lower bound underestimates $\Delta S_{ads,aq}$ and the upper bound closely agrees with the experimental value. This contrasts to the binding mode of alcohol in the vacuum phase at low coverages, where weak physisorption between the Pt surface and aliphatic chain leads to a horizontal adsorption.[59] However, in the aqueous phase, the desorption of water is enthalpically disfavoured due to the strong chemisorption of Pt-H_2O compared to physisorbed Pt-CH_X. Therefore we propose the carbon chain remains orthogonal to the Pt surface, in full interaction with the solvent phase. However, the lattice statistics model of *Bockris et al.*[58] which constructs the θ-Voltage curve of the Pt(111)/organic interface predicts the converse. The discrepancy between the model presented in this study and the prediction of *Bockris et al.* could arise from either an error within their model or an additional source of entropy loss unaccounted for in our approach. With further experimental data, we believe the model presented in this study has potential to provide geometric insights into the binding of small organic molecules to the metallic surface with minimal computational cost.

Table 1: Entropy of adsorption values in the gaseous and aqueous phase. Lower bound (LB) calculcated by statistical mechanical arguments and accentric factor approximations of the cavitation entropy. Upper bound (UB) calculated as the entropy of fusion for the approximate number of H_2O molecules displaced based on the intersecting surface area of the metallic surface and adsorbate. All values stated in $JK^{-1}mol^{-1}$.

Molecule	$\Delta S_{g,ads}$	$\Delta S_{aq,ads}$ LB	$\Delta S_{aq,ads}$ UB	$\Delta S_{aq,ads}$ Expt. [26]	# H_2O Displaced
Benzaldehyde	-152	117	174	-	4.4
Benzene	-145	93	141	-	3.6
Benzoic Acid	-152	122	175	191	4.1
Cyclohexanol	-147	62	84	-	1.7
Furfural	-151	88	133	-	3.5
H2	-45	28	37	-	0.7
Naphtholic Acid	-157	198	271	254	5.5
Naphthol	-153	180	254	244	5.7
Phenol	-148	64	151	188	4.1
Butanol	-131	109	151	59	3.2
Valeric Acid	-135	131	180	81	3.7
Butanol - Vertical	-131	49	68	59	1.5
Valeric Acid - Vertical	-135	66	90	81	1.8

3.2 parameterising the Implicit Solvent of Solvation for Pt

Implicit solvent models are a powerful tool for obtaining ΔG_{solv} data at low computational cost. However, reactions at the metallic surface are physically distinct from the systems typically used to parameterise the solvent model. In order to demonstrate the necessity of reparameterising these models, we compared the values of ΔG_{ads}^{solv} obtained with a soft sphere cavity model (parameterised to give accurate value of ΔG_{solv} per atom of the Pt(111) surface) to the commonly used charge based cavity model of VASPsol.

Parameterisation of the implicit solvent model follows the method of our previous publication,[14] where the cavity radius of Pt atoms for a four layer, (7x6) Pt(111) facet are varied through a range of scale factors (f) from the default cavity radius of 2.29 Å.[46] By performing a third order polynomial fit, we obtain a value matching the experimental ΔG_{solv} of a single Pt atom at the surface. However, as there is no direct measurement of ΔG_{solv}, for the Pt(111) suerface we must approximate this value as a sum of measurements of ΔH_{solv} and $T\Delta S_{solv}$.

$\Delta H_{solv,Pt}$ was calculated as the difference between the bond energy of the solid Pt(111)/water interface ($E_{adh,Pt/H_2O_{(s)}}$) and the surface energy of solid water ($\gamma_{H_2O_{(s)}}$, renormalised to the surface area of a single Pt site), which accounts for the heat released by water upon re-entry into the bulk.

$$\Delta H_{solv,Pt} = E_{adh,Pt/H_2O_{(s)}} - \gamma_{H_2O_{(s)}} \tag{16}$$

As shown by *Singh et al.*,[24] $E_{adh,Pt/H_2O}$ can be taken as the Pt-H_2O bond energy, where it is assumed $E_{adh,Pt/H_2O_{(s)}} = E_{adh,Pt/H_2O_{(l)}}$. $E_{adh,Pt/H_2O}$ is taken as 0.32 Jm^{-2} [16] and $\gamma_{H_2O_{(s)}}$ as 0.102 Jm^{-2}, from which we obtain the change of bonding energy per unit area. Assuming a single Pt atom occupies 7.68 $\mathrm{Å}^2$ (from a lattice constant of 3.92 Å), it can be approximated that $E_{adh,Pt/H_2O_{(s)}} = 14.81$ kJ mol^{-1} and the equivalent $\gamma_{H_2O_{(s)}}$ per mol of Pt is 5.04 kJ mol^{-1}. Overall, this yields $\Delta H_{solv,Pt} = -9.76$ kJ mol^{-1} per Pt atom.

ΔS_{solv} for the Pt(111) surface has not yet been measured experimentally. As discussed in Section 3.1, there are arguments for using either the upper bound entropy values calculated with the entropy of fusion (ΔS_{fus} ie. The entropy of transition from the liquid to solid phase) or the entropic lower bound, where the accentric factor model approximates the entropy of cavitation. For each model, the entropy value for the upper bound is $\Delta S_{solv} = -5.41\ kJmol^{-1}$ and the lower bound is $\Delta S_{solv} = -2.58$ kJmol^{-1} per surface Pt(111) atom.

Overall, this yields ΔG_{solv} values of -4.35 kJmol^{-1} and -7.18 kJmol^{-1} for a single Pt molecule upper and lower entropy bounds respectively, which we then used to parameterise the implicit solvent model (Figure 2). Performing a third order polynomial fit for the values of ΔG_{solv} gives optimal values of $f = 0.904$ (lower bound entropy) and $f = 0.936$ (upper bound entropy). Table 2 shows the values of ΔG^{aq}_{ads} obtained with the two fitted values of ΔG_{solv} for a range of adsorbates. As previously discussed, the charge based model parameterised to capture the ΔG_{solv} of molecules composed of light elements is ill-suited to capture the ΔG_{solv} of heavy/metallic atoms.[14] In the case of adsorption free energies, ΔG^{aq}_{ads} increases

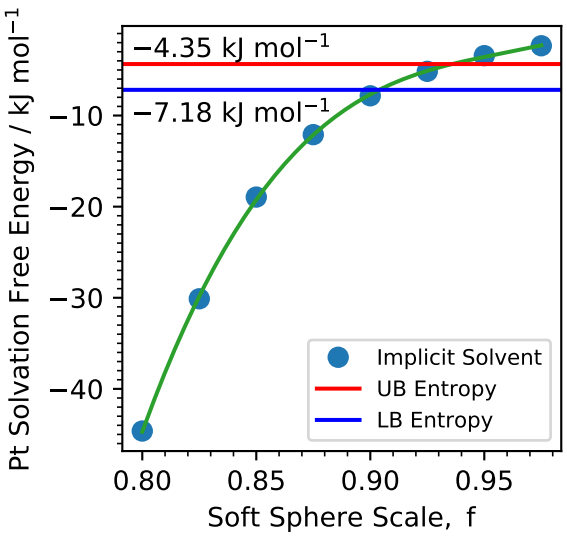

Figure 2: The change of ΔG_{solv} per Pt atom with respect to the scale factor of the default vdW radius of $r_{vdw} = 2.29$ Å of the (111) facet for a 4 layer (7×6) supercell.

or decreases very slightly relative to ΔG_{ads}^{vac} as a consequence of the cavity function creating an oversized dielectric cavity for the Pt atom. This means the negative ΔG_{solv}^{pol} contribution is small relative to the positive ΔG_{solv}^{npol}, leading to an erroneous increase in the aqueous adsorption free energy relative to the vacuum phase.

At the selected coverage ($\theta \approx 0.15$ for all aromatic species, $\theta = 0.05$ for hydrogen and $\theta = 0.09$ furfural and cyclohexanol) the correct qualitative trend of decreasing ΔG_{ads}^{aq} compared to ΔG_{ads}^{vac} is observed using the reparameterised soft sphere model. However, without considering coverage effects, adsorbate orientation or using the correct definition of the differential energy changes in solvent, there are large errors with respect to experiment. This is addressed in Section 3.3. We will briefly discuss other possible factors contributing to errors. Firstly, each molecule is adsorbed to their most stable adsorption site, when the overall adsorption energy is closer to an average of several, weaker adsorption sites.[6] This leads to an overestimation for ΔG_{ads}^{vac} of approximately 12 kJ mol^{-1} for phenol.[6] Secondly, the optB88-vdW functional is known to overbind phenol molecules to the Pt(111) by approximately 11 kJ mol^{-1} at zero coverage.[22,60] Assuming both effects are at play in the implicit solvent calculation, this leads to an approximate overestimation of ~ 20 kJmol^{-1}. Furthermore, we

note that the definition of entropy is an approximation based on the 2D ideal gas model. This assumes that the adsorbate is at temperatures sufficiently high enough to achieve barrierless diffusion across the metallic surface. Although the 2D ideal gas formulation appears to hold at temperatures of 150 K for simple alcohols and alkanes, the strong binding between Pt(111) and aromatic molecules may further impede translational motion. Additionally, we approximate that the entropy of adsorption is equivalent in vacuum and solvent, where the changes entropy due to restrictions of movement in solvent are accounted for solely through the implicit solvent model. In theory, a portion of this entropy contributed should be accounted for by the use of well parameterised implicit solvation model, but as an untested approximation, this must still be considered as a source of error.

Under the definition of integral ΔG_{ads}^{aq} at low coverages, discrepencies of up to 100 kJ mol^{-1} occur for the molecules under study. However, across all experimental data shown in Table 2, ΔG_{ads}^{aq} becomes more exothermic relative to ΔG_{ads}^{vac}. We have shown that by reparameterising the cavity of the Pt atom while maintaining the optimized cavity parameters of the organic adsorbate, the implicit solvent model correctly replicates this trend, but further factors such as coverage, orientation and the definition of ΔG_{ads}^{aq} must be considered to achieve meaningful experimental comparisons.

Table 2: The integrated ΔG_{ads}^{aq} values for the soft sphere model, with individually parameterised cavity radius compared to the charge density based cavity model of VASPsol and experimental values of ΔG_{ads}^{aq}. All values in kJ mol^{-1}.

Molecule	$\Delta G_{ads}^{int,vac}$ (ONETEP)	$\Delta G_{ads}^{int,aq}$ (Lower Bound)	$\Delta G_{ads}^{int,aq}$ (Upper Bound)	$\Delta G_{ads}^{int,aq}$ (VASPsol)	$\Delta G_{ads}^{diff,aq}$ (Expt.)
Phenol	-195	-135	-153	-195	-9[5]
Furfural	-165	-107	-122	-146	-26.1[5]
Cyclohexanol	-65	-15	-39	-84	-17[5]
Hydrogen	-40	-31	-31	-65	+2.67[2]
Benzaldehyde	-203	-143	-162	-162	-30.5[5]
Benzene	-184	-141	-157	-201	-

3.3 Coverage Effects

Using increasing coverages by varing the cell size and number of adsorbates, we investigated the change in adsorption free energy in solvent. The geometries at each coverage are shown in SI S4.

Table 3: Linear fits to the Temkin isotherm of adsorbed to the Pt(111) surface according to $\Delta G^{int}_{ads,\theta} = -\Delta G^{int}_{ads,\theta=0} + b\theta$. All values in kJmol^{-1}

Adsorbate	$\Delta G^{int,vac}_{ads,\theta=0}$	b (Vacuum)	$\Delta G^{int,vac}_{ads,\theta=1}$	$\Delta G^{int,solv}_{ads,\theta=0}$	b (Solvent)	$\Delta G^{int,solv}_{ads,\theta=1}$
Hydrogen Atom	-26	16	-20	-29	12	-16
Phenol	-167	34	-133	-111	13	-98
Furfural (Flat)	-159	36	-123	-125	16	-109
Cyclohexanol (Vertical)	-26	-14	-40	+26.5	-69	-43

Table 4: The predicted $\Delta G^{diff}_{ads,\theta}$ in vacuum in solvent compared to existing experimental data. Calculated for $\theta = 1$. Implicit solvent values shown for the lower bound entropy estimate. All values in kJmol^{-1}.

Adsorbate	$\Delta G^{diff,vac}_{ads,\theta=1}$	$\Delta G^{diff,vac}_{ads,\theta}$ (Expt.)	$\Delta G^{diff,solv}_{ads,\theta=1}$	$\Delta G^{diff,solv}_{ads,\theta}$ (Expt.)
Hydrogen Atom	-5	-24[a]/-17[b]	-5	-20[a]/-15[b]
Phenol	-98	-	-86	-9[23]
Furfural	-88	-	-92	-26[5]
Cyclohexanol	-54	-	-112	-17[23]

[a] *Ab initio* MD.[2] [b] Van't-Hoff.[2]

The dissociation of H_2 in the vacuum phase ($\Delta G^{diff,vac}_{ads,\theta=1}$) compares favourably with results obtained from experiment, but underestimates the overall free energy change by 10 kJmol^{-1} (Table 4). To meaningfully compare our results with experiment, we note the values of *Yang et al.*[61] were measured relative to the gaseous reference state of H_2, whereas our results measure adsorption according to the reaction from state B to D of Scheme 1. To align the experimental values to the solvated H_2 reference state, we subtract the entropy of solvation for molecular hydrogen from the experimental and *ab initio* MD values ($\Delta S_{solv}(\frac{1}{2}H_2) = -55\ JK^{-1}mol^{-1}$ [62]).

In experiment, the overall free energy change of adsorption in the aqueous phase is 5 kJ mol^{-1} lower than vacuum. This is reflected in the implicit solvent results, where

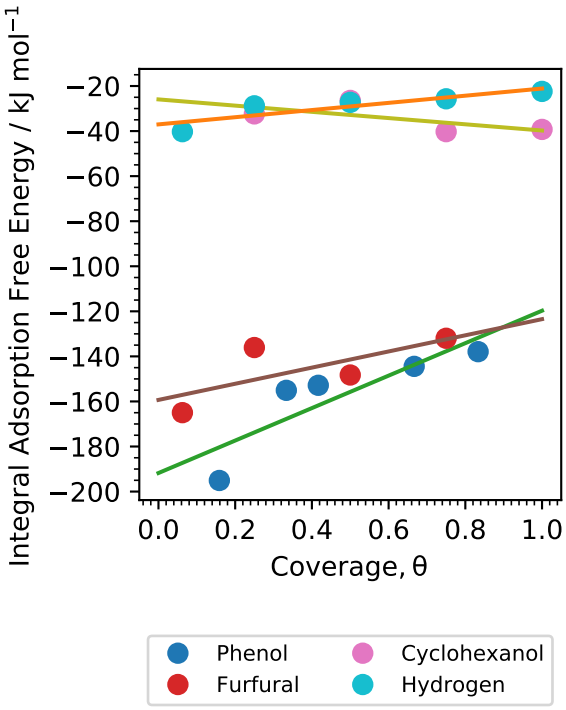

Figure 3: Integrated free energy change of adsorption in vacuum across a range of coverages on Pt(111). All coverages normalised to the respective saturation coverage of each molecule ($\theta_{sat} = 1, 0.25, 0.25, 0.15$ for hydrogen, furfural, cyclohexanol and phenol respectively). Linear fit to the Temkin isotherm $\Delta G^{int}_{ads,\theta} = \Delta G^{int}_{ads,\theta=0} + b\theta$. Horizontal geometries used for all adsorbates.

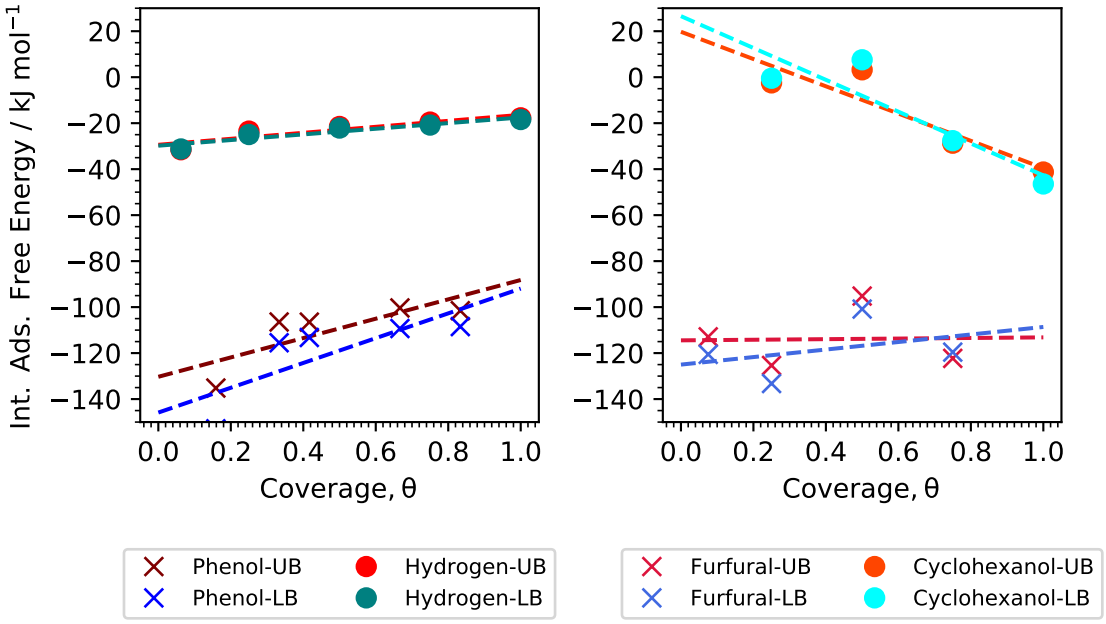

Figure 4: Integrated free energy change of adsorption in solvent across a range of coverages on Pt(111). All coverages normalised to the respective saturation coverage of each molecule ($\theta_{sat} = 1, 0.15$ for hydrogen and phenol respectively). Linear fit to the Temkin isotherm $\Delta G^{int}_{ads,\theta} = \Delta G^{int}_{ads,\theta=0} + b\theta$. Horizontal geometries used for all adsorbates apart from cyclohexanol.

$\Delta G^{int,solv}_{ads,\theta}$ relative to $\Delta G^{int,vac}_{ads,\theta}$ decreases by 5 kJmol^{-1} for the upper bound of Pt(111) solvation entropy and 9 kJmol^{-1} for the lower bound. Because b is larger in vacuum than in solvent (Table 3), $\Delta G^{diff,solv}_{ads,\theta=1}$ are very close in value despite $\Delta G^{int,solv}_{ads,\theta}$ values being consistently lower than $\Delta G^{int,vac}_{ads,\theta}$. Given these small observed changes in $\Delta G^{int,solv}_{ads,\theta}$, we propose the unfavourable dissociation of hydrogen on Pt(111) is largely driven by the insolubility of H_2 in water. AIMD techniques further support this, showing that the presence of solvent had only a minor influence on the energetics of the Pt-H bond ($\sim -2\ kJmol^{-1}$[63]). However, we note the diffusion coefficients of adsorbed H on the Pt(111) surface are lower in the aqueous phase ($D_{xy} = 7 \times 10^{-5}$cm^{2}s^{-1} *vs.* $D_{xy} = 33 \times 10^{-5}$cm^{2}s^{-1}), leading to a further reduction of entropy upon adsorption.[2] This is also accompanied by a larger decrease of the diffusion coefficient for H_2 in the first aqueous layer compared to the gas phase ($D_{xy} = 361 \times 10^{-5}$cm^{2}s^{-1} vs. $D_{xy} = 11 \times 10^{-5}$cm^{2}s^{-1}), which suggests the majority of entropy loss for H_2 results from solvation. This rationalises the large pressures required to obtain partial coverages (10 atm yields $\theta \approx 0.2$) in contrast to adsorption in the gas phase, where saturation coverage of H on Pt(111) is achieved with 0.1atm. However, without knowing the entropy of solvation of H_2 within the experimental conditions of *Yang et al.*,[2] quantitative analysis is limited.

Across the range of coverages shown, $\Delta G^{int,vac}_{ads,\theta}$ for phenol decreases linearly with increasing coverage. This agrees with literature predictions for the Temkin isotherm, where b = 70 for *ab initio* calculations of *Chaudhary et al* at the bridge sites[6] and b = 60 for gas phase calorimetry[4] measured using $\Delta H^{int,vac}_{ads,\theta}$.

As predicted in experiment, $\Delta G^{int,solv}_{ads,\theta}$ is weaker than $\Delta G^{int,vac}_{ads,\theta}$, leading to a reduction in the adsorption free energy of approximately 40 kJmol^{-1}. Furthermore, the negative correlation of adsorption free energies with respect to θ is weaker in solvent (b = 35 in solvent, b = 72 in vacuum), which is reflected in experiment where $b = 5$[23] and $b = 72$[4] for solvent and vacuum respectively. In implicit solvent, this is rationalised by the screening of repulsive interactions between the adsorbates.[64] However, we note that the value of b obtained with

the implicit solvent method is significantly larger than experimental values. This observation can be justified in one of two ways. Given the agreement of the fitted value of b in vacuum with previous *ab initio* and experimental studies, the dielectric continuum may only partially screen the repulsive intermolecular forces. We explore this possibility for a simple π-stacking interaction in the SI (S8) and find the effect of long range interactions over the range covered is small, but these effects may be sizable for greater numbers of adsorbates. Secondly, the presented geometries may not be an accurate atomistic representation of phenol adsorption with increasing coverage. For example, orientation of phenol at the Pt(111) interface may change in solvent from a horizontal to a vertical configuration. Furthermore, local high coverages have been theorised at the Pt(111) interface,[24] meaning $\Delta G^{int,solv}_{ads,\theta}$ would show little variation with higher concentrations of adsorbate and the energetics would be dominated by $\Delta G^{int,solv}_{ads,\theta=1}$. In what follows, We shall explore the former possibility in more detail.

With the presented value of b in solvent, we obtain a value of $\Delta G^{diff,solv}_{ads,\theta=1} = 98$ kJmol^{-1}, which is significantly higher than the experimentally predicted value of $\Delta G^{diff,solv}_{ads,\theta=0.5} = 9$ kJmol^{-1}. Taking the model presented *prima facie*, this suggests the horizontal binding mode of phenol incorrectly represents the adsorption of phenol in solvent. This is supported by *ab initio* MD simulation with explicit water, where the horizontal adsorption of phenol yields $\Delta G^{diff,solv}_{ads,\theta=0.4} = -151 kJmol^{-1}$ compared to $\Delta G^{diff,vac}_{ads,\theta=0.4} = -172$kJmol^{-1}.[65] This is further confirmed by classical MD simulations performed alongside our *ab initio* implicit solvent simulations, where $\Delta G^{int}_{ads,\theta=0.15} = -128$ kJmol^{-1} (See SI S6). We will explore this for furfural, where the perpendicular binding mode leads to better qualitative agreement with experimental $\Delta G^{diff,solv}_{ads,\theta=1}$.

For furfural, the first four coverage simulation are performed with the horizontal geometry and the saturation coverage calculation is performed with a perpendicular geometry (Figure 5]). Similar to phenol, we observe a large overestimation of $\Delta G^{diff,solv}_{ads,\theta=1}$ compared to experiment, and a significantly weaker value of b caused by dielectric screening. For the horizontal geometry, $\theta = 0.75$ is the saturation coverage, but full coverage of $\theta = 1.0$ nor-

malised to $\theta_{sat} = 0.25$ can be achieved using a vertical geometry, where the aromatic ring is tilted from the Pt(111) surface.

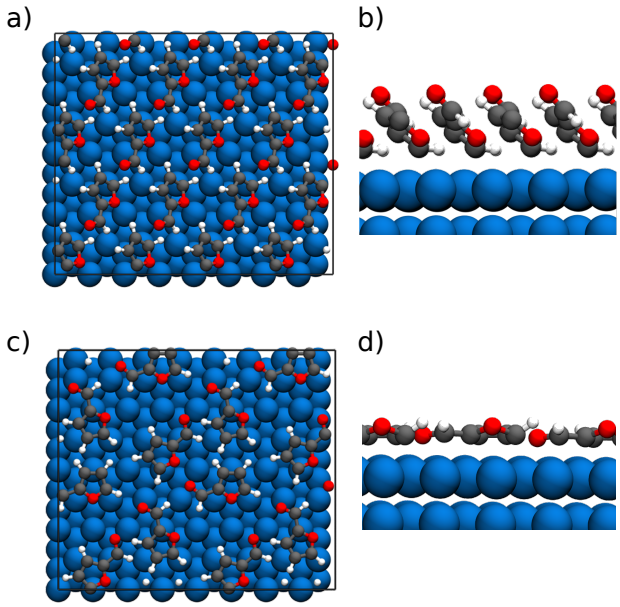

Figure 5: Geometries of furfural on the Pt(111) facet. a) and c) represent the bird's eye view of $\theta = 1.0$ vertical orientation and $\theta = 0.75$ horizontal orientations coverages. b) and c) show the same geometries viewed from the side.

At the saturation coverage, $\Delta G^{int,solv}_{ads,\theta=1} = -38$ kJmol^{-1}, which more closely aligns to the experimental value of $\Delta G^{int,solv}_{ads,\theta=1} = -26$ kJmol^{-1}, where the variation of $\Delta G^{int,solv}_{ads,\theta=1}$ with coverage is close to 0. Although we achieve better agreement with experiment using the vertical geometry, we must consider why the thermodynamically favoured horizontal configurations may not occur in electrochemical conditions. It is known the orientation of adsorbates are sensitive to a variety of conditions, such as adsorbate concentration,[66] voltage[67] and the species of electrolyte.[68] Simulations which emulate the latter two properties are possible within the implicit solvent model of ONETEP,[69,70] but are beyond the scope of this study. As we simulate adsorption for an uncharged slab (ie. at the potential of zero charge) in the absence of electrolyte, the horizontal geometry may be erroneously energetically favoured. This may further justify the discrepencies observed for phenol, where the vertical geometry may further improve agreement with experiment.

When we consider cyclohexanol, the $\Delta G_{ads,\theta}^{int,vac}$ in the vertical orientation increases with coverage, in contrast to hydrogen and horizontal phenol/furfural. Confirmation of this observation requires calorimetric data of cyclohexanol across a range of coverages.

Compared to phenol and hydrogen, the computed value of $\Delta G_{ads,\theta}^{int,solv}$ for cyclohexanol is significantly smaller than $\Delta G_{ads,\theta}^{int,vac}$ at low coverages. Especially in the lower bound entropy, adsorption in solvent is predicted to be endothermic. These effects result from the relatively weak binding of cyclohexanol to Pt (which is observed in vacuum), combined with the energetically unfavourable desolvation of the Pt surface and -OH fragments. These observations are in line with experimental findings, where cyclohexanol across the measured concentration range ($10^{-6} - 10^{-3}$M) fails to achieve saturation coverage, in contrast to other measured organic molecules.[23] The higher value of $\Delta G_{ads,\theta=1}^{int,solv}$ suggests that cyclohexanol is stable on the Pt surface at high local coverages, as is theorised for phenol adsorption in the aqueous phase.[24] This is rationalised by both the apparent attractive interactions between the cyclohexanol fragments and the exclusion of the dielectric cavity surface area, which models the favourable desolvation of the hydrophobic alkane fragment.

The large value of $b = -69$ for the adsorption of cyclohexanol in solvent compared to vacuum $b = -14$ is driven by the exclusion of the cavity surface area of the adsorbate at higher coverages. In the vertical binding mode, desolvation of the fragment exposed to the dielectric only occurs when adsorbates are within proximity of one another. At small distances, their dielectric cavities merge and the surface accessible surface area decreases, meaning $\Delta G_{ads,\theta}^{int,solv}$ becomes more exothermic.

In the limit of high local coverages, the Temkin isotherm model measured across the range of coverages shown here becomes a less useful comparison to experiment. This is because in spite of increasing the number of sites occupied with larger concentrations in experiment, the measured adsorption value of $\Delta G_{ads,\theta}^{int,solv}$ reflects that of the higher coverage values. As a result, the energetics of adsorption lead to $\Delta G_{ads,\theta}^{diff,solv} \approx \Delta G_{ads,\theta}^{int,solv}$. We note that by following this rationale, we acquire semi-quantative agreement with experiment, where the

calculated value of $\Delta G^{int,solv}_{ads,\theta} = -43$ kJmol^{-1} compares favourably with the experimental value of $\Delta G^{diff,solv}_{ads,\theta} - 17$ kJmol^{-1}.

However, an unexpected result at saturation coverage is the more exothermic value of $\Delta G^{int,solv}_{ads,\theta}$ relative to $\Delta G^{int,vac}_{ads,\theta}$. We note that the variation of $\Delta G^{int,solv}_{ads,\theta}$ for coverages $\theta = 0.25 - 1.0$ in vacuum is measured for the vertical geometry, which is known bind less strongly than the in vacuum. Performing a vacuum calculation at $\theta = 0.25$, we find that $\Delta G^{int,solv}_{ads,\theta=0.25} = -58/-32$ kJmol^{-1} for the horizontal/vertical geometries respectively for cyclohexanols. Therefore we would expect adsorption in the solvent phase to be disfavoured relative to vacuum for all molecules.

Here we have shown, provided the correct definition of $\Delta G^{solv}_{ads,\theta}$ is used, on can obtain reasonable values for the free energy of adsorption in the aqueous phase. The errors shown are on a scale of $10-30$ kJmol^{-1}, which contrasts with charge density based models where errors can increase up to 100 kJmol^{-1} as demonstrated in Table 2. The statistical thermodynamic approximations of adsorption[19] and solvation[18] entropies, combined with the flexibility of the soft sphere[10] allow for the design of an inexpensive computational model, which can semi-quantitively capture the energetics of the adsorption process at an atomistic level.

4 Conclusions

In this work, we have shown that inexpensive implicit solvent models can reproduce experimental adsorption free energies for small organic molecules in solvent. parameterisation requires separate dielectric cavity definitions for the metallic surface, achieved through the soft sphere model.[10] In contrast, isocontour charge density based cavity models are unsuitable for this purpose. Furthermore, we have shown in the absence of direct experimental measurements of ΔG_{solv} for the surface, approximations of ΔH_{solv} and ΔS_{solv} yield semi-quantitative results for the overall ΔG_{solv}. We find simple approximations based on either the ice-like bilayer model[48] or the accentric cavity model [18] provide a reasonable upper and

bound for ΔS_{solv}. However, a greater body of experimental data is required to validate which bound better describes the entropy of solvation for the surface. In this case, the difference between the upper and lower bound in the calculation of ΔG_{ads}^{solv} is small (~ 10 kJmol^{-1}), but this error necessarily increases with temperature and the surface area of the adsorbate. In the absence of experimental data, we predict ΔH_{solv} can be reasonably calculated through *ab initio* values of ΔH_{ads} of water to the chosen interface and the water surface energy.[16,24] If this is unavailable, we have shown that the parameterising against the change of work function in solvent may act as a reasonable guess for ΔG_{solv}.[14] As such, these methods can be easily extended to other metallic surfaces provided the above quantities are known.

In addition, we have emphasised the importance of correctly accounting for coverage effects when comparing to experimental data. We also present the utility of the entropy approximation and overall values of ΔG_{ads}^{solv} in predicting structural information for the Pt(111)/Adsorbate interface in water. Commonly in the literature, it is assumed that oxygenated aromatics adsorb horizontally to the Pt(111) surface in the aqueous phase much like in the vacuum phase. We propose that a far more likely, as shown by the results here and previous *ab initio* MD studies[65] that compounds such as phenol and furfural adsorb horizontally to the Pt(111) surface under electrochemical conditions. Our findings also support the presence of high local coverages of the adsorbates at the aqueous Pt(111) interface,[24] as shown by the relatively high values of ΔG_{ads}^{solv} predicted at saturation coverage for cyclohexanol. However, we note that a lack of atomistic understanding of adsorption in the aqueous phase makes facile comparison with experiment difficult. In an area where experimental data is limited and difficult to measure, the proposed techniques provide an inexpensive toolset for validation and prediction of ΔG_{ads}^{solv} and ΔS_{ads}^{solv} on solvated metallic surfaces. However, more statistically significant validation requires more empirical measurements for the aqueous entropy/free energy of adsorption.

Acknowledgement

G.B. (partial support), V.-A.G., M.-T.N., and R.R. were supported by the U.S. Department of Energy, Office of Science, Basic Energy Sciences, Chemical Sciences, Geo-sciences, and Biosciences Division. Computer resources were provided by Research Computing at Pacific Northwest National Laboratory (PNNL) and the National Energy Research Scientific Computing Center (NERSC), a U.S.Department of Energy Office of Science User Facility operated under Contract No. DE-AC02-05CH11231. PNNL is operated by Battelle for the U.S. Department of Energy under Contract DE-AC05-76RL01830. G.B. acknowledges the EPSRC for partial support in PhD funding. The authors acknowledge the use of the IRIDIS High Performance Computing Facility (IRIDIS 5) and associated support services at the University of Southampton in the completion of this work. We are grateful to the UK Materials and Molecular Modeling Hub (Young HPC) for computational resources, which is partially funded by EPSRC (EPSRC Grant Number: EP/T022213/1), and to the UKCP consortium for access to the ARCHER2 supercomputer (EPSRC Grant Number: EP/P022030/1)

Supporting Information Available

The supporting information describes the definitions of entropy expressed throughout this work (S1-S3), depictions of the geometries of adsorption at various coverages (S4), additional AIMD and MD simulations performed in support of this work (S5-S7), measurements of the π stacking interaction between two benzenes in the solvent phase (S8), the tabulated values of intermediate quantities used to describe the entropies of adsorption (S9) and the tabulated values of the enthalpies and free energies of adsorption in the aqueous and vacuum phase for all coverages and adsorbates (S10).

References

(1) Singh, N.; Nguyen, M. T.; Cantu, D. C.; Mehdi, B. L.; Browning, N. D.; Fulton, J. L.; Zheng, J.; Balasubramanian, M.; Gutiérrez, O. Y.; Glezakou, V. A.; Rousseau, R.; Govind, N.; Camaioni, D. M.; Campbell, C. T.; Lercher, J. A. Carbon-supported Pt during aqueous phenol hydrogenation with and without applied electrical potential: X-ray absorption and theoretical studies of structure and adsorbates. *Journal of Catalysis* **2018**, *368*, 8–19.

(2) Yang, G.; Akhade, S. A.; Chen, X.; Liu, Y.; Lee, M. S.; Glezakou, V. A.; Rousseau, R.; Lercher, J. A. The Nature of Hydrogen Adsorption on Platinum in the Aqueous Phase. *Angewandte Chemie - International Edition* **2019**, *58*, 3527–3532.

(3) Varghese, J. J.; Mushrif, S. H. Origins of complex solvent effects on chemical reactivity and computational tools to investigate them: a review. *Reaction Chemistry & Engineering* **2019**, *4*, 165–206.

(4) Carey, S. J.; Zhao, W.; Mao, Z.; Campbell, C. T. Energetics of Adsorbed Phenol on Ni(111) and Pt(111) by Calorimetry. *Journal of Physical Chemistry C* **2019**, *123*, 7627–7632.

(5) Akinola, J.; Barth, I.; Goldsmith, B. R.; Singh, N. Adsorption Energies of Oxygenated Aromatics and Organics on Rhodium and Platinum in Aqueous Phase. *ACS Catalysis* **2020**, *10*, 4929–4941.

(6) Chaudhary, N.; Hensley, A.; Collinge, G.; Wang, Y.; McEwen, J. S. Coverage-Dependent Adsorption of Phenol on Pt(111) from First Principles. *Journal of Physical Chemistry C* **2019**, *124*, 356–362.

(7) Tomasi, J.; Mennucci, B.; Cammi, R. Quantum mechanical continuum solvation models. *Chemical Reviews* **2005**, *105*, 2999–3093.

(8) Lee, M. S.; Olson, M. A. Comparison of volume and surface area nonpolar solvation free energy terms for implicit solvent simulations. *Journal of Chemical Physics* **2013**, *139*, 044119.

(9) Wang, X.; Deng, B.; Sun, Z. Thermodynamics of helix formation in small peptides of varying length in vacuo, in implicit solvent, and in explicit solvent. *Journal of Molecular Modeling* **2019**, *25*, 1–18.

(10) Fisicaro, G.; Genovese, L.; Andreussi, O.; Mandal, S.; Nair, N. N.; Marzari, N.; Goedecker, S. Soft-Sphere Continuum Solvation in Electronic-Structure Calculations. *Journal of Chemical Theory and Computation* **2017**, *13*, 3829–3845.

(11) Zhang, J.; Zhang, H.; Wu, T.; Wang, Q.; Van Der Spoel, D. Comparison of Implicit and Explicit Solvent Models for the Calculation of Solvation Free Energy in Organic Solvents. *Journal of Chemical Theory and Computation* **2017**, *13*, 1034–1043.

(12) Iyemperumal, S. K.; Deskins, N. A. Evaluating Solvent Effects at the Aqueous/Pt(111) Interface. *ChemPhysChem* **2017**, *18*, 2171–2190.

(13) van der Spoel, D.; Zhang, J.; Zhang, H. Quantitative predictions from molecular simulations using explicit or implicit interactions. *WIREs Computational Molecular Science* **2021**, 1560.

(14) Bramley, G.; Nguyen, M.-T.; Glezakou, V.-A.; Rousseau, R.; Skylaris, C.-K. Reconciling Work Functions and Adsorption Enthalpies for Implicit Solvent Models: A Pt (111)/Water Interface Case Study. *Journal of Chemical Theory and Computation* **2020**, *16*, 2703–2715.

(15) Saleheen, M.; Heyden, A. Liquid-Phase Modeling in Heterogeneous Catalysis. *ACS Catalysis* **2018**, *8*, 2188–2194.

(16) Rumptz, J. R.; Campbell, C. T. Adhesion Energies of Solvent Films to Pt(111) and Ni(111) Surfaces by Adsorption Calorimetry. *ACS Catalysis* **2019**, *9*, 11819–11825.

(17) Heenen, H. H.; Gauthier, J. A.; Kristoffersen, H. H.; Ludwig, T.; Chan, K. Solvation at metal/water interfaces: An ab initio molecular dynamics benchmark of common computational approaches. *The Journal of Chemical Physics* **2020**, *152*, 144703.

(18) Garza, A. J. Solvation Entropy Made Simple. *Journal of Chemical Theory and Computation* **2019**, *15*, 3204–3214.

(19) Campbell, C. T.; Sellers, J. R. V. The Entropies of Adsorbed Molecules. *Journal of the American Chemical Society* **2012**, *134*, 18109–18115.

(20) Collinge, G.; Yuk, S. F.; Nguyen, M.-T.; Lee, M.-S.; Glezakou, V.-A.; Rousseau, R. Effect of Collective Dynamics and Anharmonicity on Entropy in Heterogenous Catalysis: Building the Case for Advanced Molecular Simulations. *ACS Catalysis* **2020**, *10*, 9236–9260.

(21) Jørgensen, M.; Grönbeck, H. Adsorbate Entropies with Complete Potential Energy Sampling in Microkinetic Modeling. *The Journal of Physical Chemistry C* **2017**, *121*, 7199–7207.

(22) Wong, B. M.; Collinge, G.; Hensley, A. J.; Wang, Y.; McEwen, J. S. Benchmarking the accuracy of coverage-dependent models: adsorption and desorption of benzene on Pt (1 1 1) and Pt3Sn (1 1 1) from first principles. *Progress in Surface Science* **2019**, *94*, 100538.

(23) Singh, N.; Sanyal, U.; Fulton, J. L.; Gutiérrez, O. Y.; Lercher, J. A.; Campbell, C. T. Quantifying Adsorption of Organic Molecules on Platinum in Aqueous Phase by Hydrogen Site Blocking and in Situ X-ray Absorption Spectroscopy. *ACS Catalysis* **2019**, *9*, 6869–6881.

(24) Singh, N.; Campbell, C. T. A Simple Bond-Additivity Model Explains Large Decreases in Heats of Adsorption in Solvents Versus Gas Phase: A Case Study with Phenol on Pt(111) in Water. *ACS Catalysis* **2019**, *9*, 8116–8127.

(25) Singh, N.; Sanyal, U.; Fulton, J. L.; Gutiérrez, O. Y.; Lercher, J. A.; Campbell, C. T. Quantifying Adsorption of Organic Molecules on Platinum in Aqueous Phase by Hydrogen Site Blocking and in Situ X-ray Absorption Spectroscopy. *ACS Catalysis* **2019**, *9*, 6869–6881.

(26) Bockris, J. O.; Jeng, K. T. In-situ studies of adsorption of organic compounds on platinum electrodes. *Journal of Electroanalytical Chemistry* **1992**, *330*, 541–581.

(27) Prentice, J. C. et al. The ONETEP linear-scaling density functional theory program. *The Journal of chemical physics* **2020**, *152*, 174111.

(28) Skylaris, C.-K.; Mostofi, A. A.; Haynes, P. D.; Diéguez, O.; Payne, M. C. Nonorthogonal generalized Wannier function pseudopotential plane-wave method. *Physical Review B* **2002**, *66*, 35119.

(29) Mermin, N. D. Thermal properties of the inhomogeneous electron gas. *Physical Review* **1965**, *137*, A1441–A1443.

(30) Marzari, N.; Vanderbilt, D.; Payne, M. C. Ensemble Density-Functional Theory for ¡i¿Ab Initio¡/i¿ Molecular Dynamics of Metals and Finite-Temperature Insulators. *Physical Review Letters* **1997**, *79*, 1337–1340.

(31) Ruiz-Serrano, ; Skylaris, C.-K. A variational method for density functional theory calculations on metallic systems with thousands of atoms. *The Journal of Chemical Physics* **2013**, *139*, 054107.

(32) Dion, M.; Rydberg, H.; Schröder, E.; Langreth, D. C.; Lundqvist, B. I. Van der Waals Density Functional for General Geometries. *Physical Review Letters* **2004**, *92*, 246401.

(33) Blöchl, P. E. Projector augmented-wave method. *Physical Review B* **1994**, *50*, 17953–17979.

(34) Garrity, K. F.; Bennett, J. W.; Rabe, K. M.; Vanderbilt, D. Pseudopotentials for high-throughput DFT calculations. *Computational Materials Science* **2014**, *81*, 446–452.

(35) Hine, N. D. M.; Robinson, M.; Haynes, P. D.; Skylaris, C.-K.; Payne, M. C.; Mostofi, A. A. Accurate ionic forces and geometry optimization in linear-scaling density-functional theory with local orbitals. *Physical Review B* **2011**, *83*, 195102.

(36) Packwood, D.; Kermode, J.; Mones, L.; Bernstein, N.; Woolley, J.; Gould, N.; Ortner, C.; Csányi, G. A universal preconditioner for simulating condensed phase materials. *The Journal of Chemical Physics* **2016**, *144*, 164109.

(37) Kresse, G.; Hafner, J. Ab initio molecular dynamics for liquid metals. *Physical Review B* **1993**, *47*, 558–561.

(38) Kresse, G.; Hafner, J. Ab initio molecular-dynamics simulation of the liquid-metal–amorphous-semiconductor transition in germanium. *Physical Review B* **1994**, *49*, 14251–14269.

(39) Kresse, G.; Furthmüller, J. Efficient iterative schemes for ab initio total-energy calculations using a plane-wave basis set. *Physical Review B - Condensed Matter and Materials Physics* **1996**, *54*, 11169–11186.

(40) Mathew, K.; Sundararaman, R.; Letchworth-Weaver, K.; Arias, T. A.; Hennig, R. G. Implicit solvation model for density-functional study of nanocrystal surfaces and reaction pathways. *Journal of Chemical Physics* **2014**, *140*.

(41) Mathew, K.; Kolluru, V. S. C.; Mula, S.; Steinmann, S. N.; Hennig, R. G. Implicit self-consistent electrolyte model in plane-wave density-functional theory. *The Journal of Chemical Physics* **2019**, *151*, 234101.

(42) Kresse, G.; Joubert, D. From ultrasoft pseudopotentials to the projector augmented-wave method. *Physical Review B* **1999**, *59*, 1758–1775.

(43) Mostofi, A. A. On Linear-Scaling Methods for Quantum Mechanical First-Principles Calculations. Ph.D. thesis, University of Cambridge, 2003.

(44) Dziedzic, J.; Helal, H. H.; Skylaris, C.-K.; Mostofi, A. A.; Payne, M. C. Minimal parameter implicit solvent model for ab initio electronic structure calculations. *Arxiv preprint arXiv:1112.1268* **2011**, 1–13.

(45) Womack, J. C.; Anton, L.; Dziedzic, J.; Hasnip, P. J.; Probert, M. I.; Skylaris, C. K. DL-MG: A Parallel Multigrid Poisson and Poisson-Boltzmann Solver for Electronic Structure Calculations in Vacuum and Solution. *Journal of Chemical Theory and Computation* **2018**, *14*, 1412–1432.

(46) Alvarez, S. A cartography of the van der Waals territories. *Dalton Transactions* **2013**, *42*, 8617.

(47) Marenich, A. V.; Kelly, C. P.; Thompson, J. D.; Hawkins, G. D.; Chambers, C. C.; Giesen, D. J.; Winget, P.; Cramer, C. J.; Truhlar, D. G. *Minnesota Solvation Database - version 2012*; 2012.

(48) Akinola, J.; Singh, N. Temperature dependence of aqueous-phase phenol adsorption on Pt and Rh. *Journal of Applied Electrochemistry* **2020**, *1*, 3.

(49) Doering, D. L.; Madey, T. E. The adsorption of water on clean and oxygen-dosed Ru(011). *Surface Science* **1982**, *123*, 305–337.

(50) Ogasawara, H.; Brena, B.; Nordlund, D.; Nyberg, M.; Pelmenschikov, A.; Pettersson, L. G.; Nilsson, A. Structure and Bonding of Water on Pt(111). *Physical Review Letters* **2002**, *89*, 276102.

(51) *WebBook NIST (2017) Standard Reference Database Number 69*; National Institute of Standards and Technology: Gaithersburg MD, 2017; p 20899.

(52) Lew, W.; Crowe, M. C.; Karp, E.; Campbell, C. T. Energy of Molecularly Adsorbed Water on Clean Pt(111) and Pt(111) with Coadsorbed Oxygen by Calorimetry. *J. Phys. Chem. C* **2011**, *115*, 9164–9170.

(53) Gim, S.; Cho, K. J.; Lim, H.-K.; Kim, H. Structure, Dynamics, and Wettability of Water at Metal Interfaces. *Scientific Reports* **2019**, *9*, 14805.

(54) Dionísio, M. S.; Ramos, J. J. M.; Gonçalves, R. M. The enthalpy and entropy of cavity formation in liquids and Corresponding States Principle. *Canadian Journal of Chemistry* **1990**, *68*, 1937–1949.

(55) Gossenberger, F.; Roman, T.; Groß, A. Hydrogen and halide co-adsorption on Pt(111) in an electrochemical environment: a computational perspective. *Electrochimica Acta* **2016**, *216*, 152–159.

(56) Singh, N.; Lee, M.-S.; Akhade, S. A.; Cheng, G.; Camaioni, D. M.; Gutiérrez, O. Y.; Glezakou, V.-A.; Rousseau, R.; Lercher, J. A.; Campbell, C. T. Impact of pH on Aqueous-Phase Phenol Hydrogenation Catalyzed by Carbon-Supported Pt and Rh. *ACS Catalysis* **2019**, *9*, 1120–1128.

(57) Chen, X.; McCrum, I. T.; Schwarz, K. A.; Janik, M. J.; Koper, M. T. M. Co-adsorption of Cations as the Cause of the Apparent pH Dependence of Hydrogen Adsorption on a Stepped Platinum Single-Crystal Electrode. *Angewandte Chemie International Edition* **2017**, *56*, 15025–15029.

(58) Bockris, M.; Green, M.; J Swinkels, D. A.; Blomgren, E. A.; Jesch, C. *Relationships of Organic Compounds*; 1960; Vol. 111; p 1948.

(59) Tereshchuk, P.; Da Silva, J. L. F. Density Functional Investigation of the Adsorption of Ethanol–Water Mixture on the Pt(111) Surface. *The Journal of Physical Chemistry C* **2013**, *117*, 16942–16952.

(60) Chaudhary, N.; Hensley, A.; Collinge, G.; Wang, Y.; McEwen, J.-S. Coverage-Dependent Adsorption of Phenol on Pt(111) from First Principles. *The Journal of Physical Chemistry C* **2020**, *124*, 356–362.

(61) Yan, L.; Sun, Y.; Yamamoto, Y.; Kasamatsu, S.; Hamada, I.; Sugino, O. Hydrogen adsorption on Pt(111) revisited from random phase approximation. *The Journal of Chemical Physics* **2018**, *149*, 164702.

(62) Frank, H. S.; Evans, M. W. Free Volume and Entropy in Condensed Systems III. Entropy in Binary Liquid Mixtures; Partial Molal Entropy in Dilute Solutions; Structure and Thermodynamics in Aqueous Electrolytes. *The Journal of Chemical Physics* **1945**, *13*, 507–532.

(63) Yan, L.; Yamamoto, Y.; Shiga, M.; Sugino, O. Nuclear quantum effect for hydrogen adsorption on Pt(111). *Physical Review B* **2020**, *101*, 165414.

(64) Mao, Y.; Loipersberger, M.; Kron, K. J.; Derrick, J. S.; Chang, C. J.; Sharada, S. M.; Head-Gordon, M. Consistent inclusion of continuum solvation in energy decomposition analysis: theory and application to molecular CO2 reduction catalysts. *Chemical Science* **2021**, *12*, 1398–1414.

(65) Yoon, Y.; Rousseau, R.; Weber, R. S.; Mei, D.; Lercher, J. A. First-principles study of phenol hydrogenation on pt and ni catalysts in aqueous phase. *Journal of the American Chemical Society* **2014**, *136*, 10287–10298.

(66) Soriaga, M. P.; Hubbard, A. T. Determination of the orientation of aromatic molecules adsorbed on platinum electrodes. The effect of solute concentration. *Journal of the American Chemical Society* **1982**, *104*, 3937–3945.

(67) Li, C.-Y.; Le, J.-B.; Wang, Y.-H.; Chen, S.; Yang, Z.-L.; Li, J.-F.; Cheng, J.; Tian, Z.-Q. In situ probing electrified interfacial water structures at atomically flat surfaces . *Nature Materials* **2019**, *18*, 697–701.

(68) Soriaga, M. P.; White, J. H.; Song, D.; Hubbard, A. T. Adsorption and orientation of aromatic compounds at smooth polycrystalline platinum electrodes: The effect of halide electrolytes. *Journal of Electroanalytical Chemistry and Interfacial Electrochemistry* **1984**, *171*, 359–363.

(69) Bhandari, A.; Peng, C.; Dziedzic, J.; Anton, L.; Owen, J. R.; Kramer, D.; Skylaris, C.-K. Electrochemistry from first-principles in the grand canonical ensemble. *The Journal of Chemical Physics* **2021**, *155*, 24114.

(70) Dziedzic, J.; Bhandari, A.; Anton, L.; Peng, C.; Womack, J. C.; Famili, M.; Kramer, D.; Skylaris, C.-K. Practical Approach to Large-Scale Electronic Structure Calculations in Electrolyte Solutions via Continuum-Embedded Linear-Scaling Density Functional Theory. *The Journal of Physical Chemistry C* **2020**, *124*, 7860–7872.